

Higher Accuracy through Combining of quasi-3D (instead of 1D) with true-3D Manifold Flow Models during the Simulation of ICE Gas Exchange Processes

Victor Gheorghiu

Mechanical Engineering, University of Applied Sciences
Hamburg, Germany

Copyright © 2001 Society of Automotive Engineers, Inc.

ABSTRACT

So far the simulation of the gas exchange, air/fuel mixture formation and burning processes in ICE was usually done, for cost reasons, by a combination of 1D models for the intake and exhaust manifold and 3D models for the cylinder. In order to implement the modeling of the pipe flow more exactly and also economically at the same time, a new method is presented here, called the **quasi-3D method**.

After the presentation of the theoretical basis and the detailed description of the modeling technique, the quasi-3D method for one-cylinder research engine is applied. The simulation results of this application are compared with pressure measurements, followed by an evaluation and discussion of their accuracy.

INTRODUCTION

To estimate the required initial conditions for the simulation of the cylinder air/fuel mixture formation and burning processes, one must have knowledge about the quantity, the composition and the flow-field of the intake charge.

Since the computation costs are high for the implementation of the three-dimensional (3D) simulations of the gas exchange processes due to the large number of discretization elements needed for the manifolds shape, one-dimensional (1D) simulations are used instead. In this case, since the 1D-simulation of the gas flow processes cannot describe the whole reality (i.e. the three-dimensionality) of the gas flow correctly, curvatures, asymmetry of the pipes and channels in the simulation are disregarded.

In order to find a compromise procedure for this situation, a new method is presented that improves the quality of the 1D-simulation results noticeably without increasing the cost of computation proportionally. This method is referred to as the **quasi-3D method** in the following. It is

based on the 1D partial differential equations (PDEs), which model the unsteady compressible flow process of a viscous fluid, and it is introduced now in the following steps:

1. The 3D flow equations are deduced appropriately, as to consider the distortion of the velocity distribution (size and direction) in each pipe cross-section. Their integration over the pipe cross-section results in the 1D flow equations, the terms of which still contain integrals of the velocity distribution. In the following these integrals are designated as **adjustment coefficients** of the 1D flow, since they describe the 3D distribution of the gas flow velocity. The 1D flow equations together with the adjustment coefficients form **the quasi-3D PDEs**.
2. The adjustment coefficients are further treated as temporally independent parameters in each pipe cross-section. For integration of the quasi-3D PDEs the total variation diminishing (TVD) finite difference method (as example) is used. The quasi-3D PDEs are processed accordingly here, and the application of the TVD procedure is presented in detail.
3. The determination of the adjustment coefficients, which consider the three-dimensionality of the gas flow, take place with the help of a 3D-simulation. Programs such as KIVA 3, STAR CD, FIRE, Flow-3D etc. can be used for this simulation. The 3D-simulation is only done for stationary forward and reverse flow through the pipes. The resulted 3D flow velocity fields are appropriately processed to produce the requested adjustment coefficients.
4. The quasi-3D method can be used for the accurate simulation of manifold flow processes throughout the full engine cycle. Thus can be determined the crank angle (CA) variations of the flow velocity, pressure, density and gas composition in the cylinder interfaces and the cylinder initial conditions.
5. The flow velocity CA-variations together with the adjustment coefficients enable determination of the 3D

flow velocity distributions related to CA in the cylinder interfaces. These results together with the CA-variations of the pressure, density and gas composition build the boundary conditions for the true-3D cylinder processes simulation.

Apart from the theoretical basics, which are the topic of this report, the quasi-3D method is applied (as an example) to a one-cylinder research diesel engine. The comparison between simulation results in intake pipe and cylinder and pressure measurements in multi-point intake pipe at several engine speeds and loads is shown and commented in detail.

MAIN SECTION

1. DERIVATION OF THE QUASI-3D PDEs

For the theoretical development of the 1D PDEs it is helpful to use the **stream thread notion**. In this case the lateral surface of the stream thread is impermeable to matter, since this area itself is formed by streamlines.

The classical stream thread notion is generally characterized as follows: *The variations of all state variables in the cross direction of a stream thread are much lower than in its longitudinal direction* [1]. The **quasi-3D stream thread notion** supplements the classical one by accepting that the *flow velocity varies significant in the cross direction too*.

In case of a pipe flow, since the tube wall (similar to the lateral surface of the stream thread) is impermeable to matter, the quasi-3D stream thread notion can be put into practice perfectly. This notion has the advantage that one can take into account the effect of the interior curvatures, asymmetry etc. of the pipes and channels on the resulting distorted velocity field.

1.1. Continuity equation

The continuity equation for a fluid element of the volume V (control volume), whose density is ρ , is

$$\frac{d}{dt} \left(\int_{V(t)} \rho \cdot dV \right) = 0, \quad (1)$$

in which t is time. With the help of the Gauss law one can expand the LH member of equation (1) to

$$\frac{d}{dt} \left(\int_{V(t)} \rho \cdot dV \right) = \left(\int_{V(t)} \rho \cdot dV \right)_t + \int_{S(t)} \rho \cdot (\vec{v} \cdot \vec{n}) \cdot dS, \quad (2)$$

in which the local flow velocity vector \vec{v} and the normal vector \vec{n} to the surface S of the fluid element are scalar

multiplied, and the subscript t denotes partial differentiating with respect to time.

Since the lateral surface is impermeable to matter, the final integral from equation (2) takes into consideration only the cross-section A of the stream thread. The scalar product $\vec{v} \cdot \vec{n}$ to the cross-section A is identical to the local axial flow velocity c . Thus, the continuity equation (2) becomes

$$\int_x \left(\int_{A(t)} \rho \cdot dA \right)_t \cdot dx + \int_{A(t)} \rho \cdot c \cdot dA = 0, \quad (3)$$

and after partial differentiating with respect to x , indicated by the subscript x , one results

$$\left(\int_{A(t)} \rho \cdot dA \right)_t + \left(\int_{A(t)} \rho \cdot c \cdot dA \right)_x = 0. \quad (4)$$

Now the average value of the local axial flow velocity c over the cross-section A is defined as

$$C = \frac{1}{A} \cdot \int_{A(t)} c \cdot dA. \quad (5)$$

Following the stream thread notion, the density is constant in any cross-section of the stream thread. The continuity equation becomes

$$(\rho \cdot A)_t + (\rho \cdot C \cdot A)_x = 0. \quad (6)$$

Note: In equation (6) one can replace the density ρ with any other scalar variable Y , therefore

$$(Y \cdot A)_t + (Y \cdot C \cdot A)_x = 0. \quad (7)$$

1.2. Momentum equation along the stream thread axis

This equation (Euler motion equation) for a fluid element expresses the principle of momentum conservation, i.e. the momentum variation of the fluid element is caused by the mass forces \vec{G} (such as gravitation or centrifugal) and by the forces \vec{P} that only apply to the surfaces of the fluid element.

$$\frac{d}{dt} \int_{V(t)} \rho \cdot \vec{v} \cdot dV = \int_{V(t)} \vec{G} \cdot dV + \int_{S(t)} \vec{P} \cdot dS \quad (8)$$

This vectorial equation is now projected upon the stream thread axis. By means of the Gauss law the LH member becomes

$$\frac{d}{dt} \left(\int_{V(t)} \mathbf{r} \cdot \mathbf{c} \cdot dV \right) = \left(\int_{V(t)} \mathbf{r} \cdot \mathbf{c} \cdot dV \right)_t + \int_{A(t)} \mathbf{r} \cdot \mathbf{c} \cdot (\vec{v} \cdot \vec{n}) \cdot dA \quad (9)$$

The gas exchange simulation neglects the mass forces \vec{G} as usual

$$\int_{V(t)} \vec{G} \cdot dV = 0. \quad (10)$$

The \vec{P} forces are produced from the pressure and the friction. Thus the RH member of the equation (8) becomes

$$- \int_{A(t)} p \cdot dA - \int_x \frac{I_D}{D_H} \cdot \frac{\mathbf{r} \cdot \mathbf{C} \cdot |\mathbf{C}|}{2} \cdot A \cdot dx, \quad (11)$$

in which I_D is the wall friction coefficient and D_H is the hydraulic diameter of the pipe. Inserting (9), (10) and (11) into equation (8), partially differentiating with respect to x and integrating over the cross-section A gives

$$\left(\mathbf{r} \cdot \int_{A(t)} \mathbf{c} \cdot dA \right)_t + \left(\mathbf{r} \cdot \int_{A(t)} \mathbf{c}^2 \cdot dA \right)_x = - p_x \cdot A - \frac{I_D}{D_H} \cdot \frac{\mathbf{r} \cdot \mathbf{C} \cdot |\mathbf{C}|}{2} \cdot A. \quad (12)$$

For simplifying equation (12) the well-known *Coefficient of Boussinesq* \mathbf{b} is now introduced (s. [2], [3])

$$\mathbf{b} = \frac{1}{\mathbf{C}^2 \cdot A} \cdot \int_{A(t)} \mathbf{c}^2 \cdot dA. \quad (13)$$

Thus the momentum equation along the stream thread axis becomes

$$\left(\mathbf{r} \cdot \mathbf{C} \cdot A \right)_t + \left(\mathbf{b} \cdot \mathbf{r} \cdot \mathbf{C}^2 \cdot A \right)_x = - p_x \cdot A - \frac{I_D}{D_H} \cdot \frac{\mathbf{r} \cdot \mathbf{C} \cdot |\mathbf{C}|}{2} \cdot A, \quad (14)$$

or in its conservation form

$$\left(\mathbf{r} \cdot \mathbf{C} \cdot A \right)_t + \left(\mathbf{b} \cdot \mathbf{r} \cdot \mathbf{C}^2 \cdot A + p \cdot A \right)_x = p \cdot A_x - \frac{I_D}{D_H} \cdot \frac{\mathbf{r} \cdot \mathbf{C} \cdot |\mathbf{C}|}{2} \cdot A. \quad (15)$$

1.3. Energy equation

Here one must note that the specific kinetic energy of the fluid element refers to the local flow velocity \vec{v} and not to its axial part c . This equation becomes

$$\frac{d}{dt} \left(\int_{V(t)} \left(e + \frac{\mathbf{r} \cdot \mathbf{v}^2}{2} \right) \cdot dV \right) = \int_{A(t)} \vec{P} \cdot \vec{c} \cdot dA + \int_{V(t)} \vec{G} \cdot \vec{c} \cdot dV + \int_{S(t)} q \cdot dS. \quad (16)$$

Herein e is the internal energy per unit volume and q the heat flow density across the lateral surface S of the fluid element. Interior heat sources or thermal conduction of the fluid along the stream thread remain neglected. After partial differentiation with respect to x and after integrating all terms over the cross-section A results

$$\left[A \cdot \left(e + \mathbf{g} \cdot \frac{\mathbf{r} \cdot \mathbf{C}^2}{2} \right) \right]_t + \left[A \cdot \mathbf{C} \cdot \left(e + \mathbf{a} \cdot \frac{\mathbf{r} \cdot \mathbf{C}^2}{2} \right) \right]_x = - (A \cdot \mathbf{C} \cdot p)_x + \frac{I_D}{D_H} \cdot \frac{\mathbf{r} \cdot |\mathbf{C}^3|}{2} \cdot A + \frac{4 \cdot q}{D_H} \cdot A. \quad (17)$$

In order to describe the effect of the flow velocity distribution distortion in the stream thread cross-section A on the variation of the specific kinetic energy the following coefficients are introduced

$$\mathbf{g} = \frac{1}{\mathbf{C}^2 \cdot A} \cdot \int_{A(t)} v^2 \cdot dA, \quad (18)$$

$$\mathbf{a} = \frac{1}{\mathbf{C}^3 \cdot A} \cdot \int_{A(t)} v^2 \cdot c \cdot dA. \quad (19)$$

Note: If one wants to insert the axial flow velocity c into equation (16) instead of the local flow velocity \vec{v} , i.e. if one wants to assume that the flow velocity is directed only along the stream thread axis, then the coefficients \mathbf{b} and \mathbf{g} will have identical calculation formulas. Although their formulas are identical, their physical meanings remain very different. In this case the coefficient \mathbf{a} also becomes simpler and thus identical to the well-known *Coefficient of Coriolis* (s. [3], [4]).

The coefficients \mathbf{a} , \mathbf{b} and \mathbf{g} are always greater than one. These are designated as **adjustment coefficients** of the 1D flow, since they describe the 3D distortion of the gas flow velocity field in a cross-section A of the stream thread, respectively, of the pipe.

The equation (17) can be processed now with the help of the thermal and caloric state equations of the working fluid. As an example, the fluid is regarded here as a thermally and calorically ideal gas. The suitable thermal (20) and caloric (21) equation of state provide the following for the specific internal energy e of the fluid element

$$\frac{p}{r} = R_G \cdot T \quad (20)$$

$$e = c_v \cdot T \cdot r = \frac{R_G}{k-1} \cdot T \cdot r = \frac{p}{k-1} \quad (21)$$

and thus equation (17) becomes

$$\left[A \cdot \left(\frac{p}{k-1} + g \cdot \frac{r \cdot C^2}{2} \right) \right]_t + \left[A \cdot C \cdot \left(\frac{k \cdot p}{k-1} + a \cdot \frac{r \cdot C^2}{2} \right) \right]_x = \frac{I_D}{D_H} \cdot \frac{r \cdot |C^3|}{2} \cdot A + \frac{4 \cdot k}{D_H} \cdot (T_W - T) \cdot A, \quad (22)$$

in which k means the isentropic exponent, R_G the gas constant, k the heat transfer coefficient, T the gas temperature and T_W the wall temperature.

1.4. Continuity equation for a gas component in the absence of chemical reactions

If the mass fraction r of a gas component i in a gas mixture is defined as

$$r_i = \frac{r_i}{r} \quad (23)$$

the continuity equation of this component according to equation (7) gives

$$(r_i \cdot r \cdot A)_t + (r_i \cdot r \cdot C \cdot A)_x = 0. \quad (24)$$

For example one gas component could be the exhaust gas or the gasoline vapor in a mixture of fresh charge and exhaust gas.

1.5. Conservation form of all PDEs

The PDEs represented above can be brought together in a vectorial form as equation (25) shows. The first bracket here is the temporal variation of the specific state variables of the fluid element, the second includes the convection terms of these state variables and the third the so-called source terms.

$$\left[\begin{array}{c} r \cdot A \\ r \cdot C \cdot A \\ A \cdot \left(\frac{p}{k-1} + g \cdot \frac{r \cdot C^2}{2} \right) \\ r_i \cdot r \cdot A \end{array} \right]_t +$$

$$\left[\begin{array}{c} r \cdot C \cdot A \\ A \cdot (b \cdot r \cdot C^2 + p) \\ A \cdot C \cdot \left(\frac{k \cdot p}{k-1} + a \cdot \frac{r \cdot C^2}{2} \right) \\ r_i \cdot r \cdot C \cdot A \end{array} \right]_x = \quad (25)$$

$$\left[\begin{array}{c} 0 \\ p \cdot A_x - \frac{I_D}{D_H} \cdot \frac{r \cdot C \cdot |C|}{2} \cdot A \\ \frac{I_D}{D_H} \cdot \frac{r \cdot |C^3|}{2} \cdot A + \frac{4 \cdot k}{D_H} \cdot (T_W - T) \cdot A \\ 0 \end{array} \right]$$

Since the pipe cross-section A is not a state variable, its partial derivatives can be taken from the LH into the RH member. The vectorial form of the equation (25) permits a still simpler mathematical representation, in which the square brackets can be replaced by the vectors \mathbf{U} , \mathbf{F} and \mathbf{H}

$$\mathbf{U}_t + \mathbf{F}_x = \mathbf{H}, \quad (26)$$

where

$$\mathbf{U} = \left[\begin{array}{c} r \\ r \cdot C \\ \frac{p}{k-1} + g \cdot \frac{r \cdot C^2}{2} \\ r_i \cdot r \end{array} \right] \quad (26.1)$$

$$\mathbf{F} = \left[\begin{array}{c} r \cdot C \\ b \cdot r \cdot C^2 + p \\ C \cdot \left(\frac{k \cdot p}{k-1} + a \cdot \frac{r \cdot C^2}{2} \right) \\ r_i \cdot r \cdot C \end{array} \right] \quad (26.2)$$

$$\mathbf{H} = \left[\begin{array}{c} \frac{-r}{A} \cdot (A_t + C \cdot A_x) \\ \frac{-r \cdot C}{A} \cdot \left((A_t + b \cdot C \cdot A_x) + \frac{I_D}{D_H} \cdot \frac{|C|}{2} \cdot A \right) \\ H_3 \\ \frac{-r_i \cdot r}{A} \cdot (A_t + C \cdot A_x) \end{array} \right] \quad (26.3)$$

with

$$H_3 = \frac{-1}{k-1} \cdot (A_t + k \cdot C \cdot A_x) \cdot \frac{p}{A} - \frac{r \cdot C^2}{2} \cdot \left(\frac{g \cdot A_t + a \cdot C \cdot A_x}{A} - \frac{I_D}{D_H} \cdot |C| \right) + \frac{4 \cdot k}{D_H} \cdot (T_W - T).$$

If all terms in the vector \mathbf{H} would be zero, the equation (26) becomes a homogeneous PDE, i.e.

$$\mathbf{U}_t + \mathbf{F}_x = \mathbf{0}. \quad (27)$$

2. NUMERICAL INTEGRATION OF QUASI-3D PDEs BY THE FINITE DIFFERENCE METHOD

At present there are three well-known methods for the numerical integration of the above PDEs: the finite-difference, the finite-element and the finite-volume methods. Each of these methods contains a set of specialized procedures.

In this case the finite-difference method with the so-called total variation diminishing (TVD) method, Lax-Friedrichs non-MUSCL (monotonic upstream schemes for conservation laws) approach for the homogeneous PDE (27) is used [5]. In order to consider the effect of the source terms from the vector \mathbf{H} , the TVD technique is integrated in a predictor-corrector procedure.

2.1. Processing of the homogeneous PDE (27)

For the application of the explicit Lax-Friedrichs non-MUSCL approach the homogeneous PDE (27) must be appropriately processed.

The vector \mathbf{F} can be expressed as a function of the vector \mathbf{U} components U_k , with $k=1..4$. For this purpose the density r , the average axial speed C and the pressure p are processed first

$$r = U_1, \quad C = \frac{U_2}{U_1}, \quad p = (k-1) \cdot \left(U_3 - \frac{g}{2} \cdot \frac{U_2^2}{U_1} \right).$$

This gives for \mathbf{F}

$$\mathbf{F} = \begin{bmatrix} U_2 \\ (k-1) \cdot U_3 + \left(b - \frac{k-1}{2} \cdot g \right) \cdot \frac{U_2^2}{U_1} \\ \frac{U_2}{U_1} \cdot \left(k \cdot U_3 + \frac{a-k}{2} \cdot g \cdot \frac{U_2^2}{U_1} \right) \\ \frac{U_2}{U_1} \cdot U_4 \end{bmatrix}, \quad (28)$$

and the equation (27) becomes

$$\mathbf{U}_t + \mathbf{F}(\mathbf{U})_x = \mathbf{0}. \quad (29)$$

The equation (29) is discretized now with the help of the finite-difference method along the time axis t and the space axis x . Let \mathbf{U}_j^n be the numerical approximation of the solution of equation (29) at $x = j \cdot \mathbf{D}x$ and $t = n \cdot \mathbf{D}t$, with $\mathbf{D}x$ being the spatial mesh size (equally spaced, for simplicity) and $\mathbf{D}t$ the time step.

After the application of the finite-difference method in an explicit technique the result for the homogeneous PDE (29) is

$$\mathbf{U}_j^{n+1} = \mathbf{U}_j^n - \mathbf{I} \cdot \left(\mathbf{F}_{j+\frac{1}{2}}^n - \mathbf{F}_{j-\frac{1}{2}}^n \right), \quad (30)$$

whereas the subscript $j \pm \frac{1}{2}$ points at the middle positions between j and $j \pm 1$. The mesh discretization parameter is

$$\mathbf{I} = \frac{\mathbf{D}t}{\mathbf{D}x}, \quad (31)$$

with $\mathbf{D}t$ and $\mathbf{D}x$ being the respective increments on the time and stream thread axes. The vector \mathbf{U} at the time $n+1$ here is the unknown quantity. In order to determine it, one must first determine the vector \mathbf{F} , i.e. the numerical flux, at the positions $j \pm \frac{1}{2}$.

A numerical scheme belongs to the TVD techniques, if the total variation (TV) of the state vector \mathbf{U} from the homogeneous PDE (27) in all discretization points j and at each time n fulfills the following condition [5]

$$TV(\mathbf{U}^{n+1}) \geq TV(\mathbf{U}^n) \quad \text{with} \quad TV(\mathbf{U}^n) = \sum_{j=-\infty}^{\infty} (\mathbf{U}_{j+1}^n - \mathbf{U}_j^n).$$

2.2. Application of the Lax-Friedrichs non MUSCL scheme

In case of second order schemes, the numerical flux \mathbf{F} can be written at the position $j \pm \frac{1}{2}$ utilizing so-called local characteristics

$$\mathbf{F}_{j+\frac{1}{2}} = \frac{1}{2} \cdot \left(\mathbf{F}_j + \mathbf{F}_{j+1} + \mathbf{R}_{j+\frac{1}{2}} \cdot \mathbf{F}_{j+\frac{1}{2}} \right), \quad (32)$$

in which the product $\mathbf{R} \cdot \mathbf{F}$ is responsible for achieving the second order accuracy.

2.2.1. Derivation of the right-eigenvector matrix \mathbf{R}

In order to obtain the right-eigenvector matrix \mathbf{R} , one must first determine the Jacobian matrix \mathbf{B} of \mathbf{F}

$$\mathbf{B}(\mathbf{U}) = \frac{d}{d\mathbf{U}} \mathbf{F}(\mathbf{U}), \quad (33)$$

$$\mathbf{B} = \begin{bmatrix} 0 & 1 & 0 & 0 \\ -\left(b - \frac{k-1}{2} \cdot g \right) \cdot C^2 & B_{22} & k-1 & 0 \\ B_{31} & B_{32} & k \cdot C & 0 \\ -r_j \cdot C & r_j & 0 & C \end{bmatrix}, \quad (34)$$

where

$$B_{22} = 2 \cdot \left(b - \frac{k-1}{2} \cdot g \right) \cdot C,$$

$$B_{31} = -\frac{a^2 \cdot C}{k-1} - \left(a - \frac{1}{2} \cdot k \cdot g \right) \cdot C^3,$$

$$B_{32} = \frac{a^2}{k-1} + \left(\frac{3}{2} \cdot a - k \cdot g \right) \cdot C^2,$$

and

$$a = \sqrt{\frac{k \cdot p}{r}} = \sqrt{k \cdot R_G \cdot T} \quad (35)$$

is the local speed of sound of the ideal gas in the stream thread. The eigenvalues \mathbf{d} of the matrix \mathbf{B} are the solutions of the equation

$$\det(\mathbf{B} - \mathbf{d} \cdot \mathbf{E}) = 0, \quad (36)$$

where \mathbf{E} means here the suitable identity matrix. The adjustment coefficients a , b and g , which describe the speed distribution distortion in the cross-section A of the stream thread, make the **exact** determination of the eigenvalues of the matrix \mathbf{B} impossible.

If all these three adjustment coefficients would be set to $a = b = g = 1$ in \mathbf{B} , i.e. only a 1D-flow model would be used and the flow velocity would be uniformly distributed and adjusted only by the stream thread axis, then \mathbf{B} becomes \mathbf{B}_{1D}

$$\mathbf{B}_{1D} = \begin{bmatrix} 0 & 1 & 0 & 0 \\ -\frac{1}{2} \cdot (3-k) \cdot C^2 & (3-k) \cdot C & k-1 & 0 \\ B_{31} & B_{32} & k \cdot C & 0 \\ -r_i \cdot C & r_i & 0 & C \end{bmatrix} \quad (34)$$

where

$$B_{31} = -\frac{a^2 \cdot C}{k-1} - \left(1 - \frac{k}{2} \right) \cdot C^3$$

$$B_{32} = \frac{a^2}{k-1} + \left(\frac{3}{2} - k \right) \cdot C^2$$

Their eigenvalues would assume the following expressions

$$\mathbf{d}_1 = C - a \quad \mathbf{d}_2 = C \quad \mathbf{d}_3 = C + a \quad \mathbf{d}_4 = C \quad (37)$$

These eigenvalues show the local well-known characteristic directions and form the base e.g. for the application of the well-known *Method of Characteristics*. This method was originally introduced by Riemann [7]. It was used, as a graphical technique, by Jenny [8] to calculate flows in engine manifolds, and Seifert [9] and Benson et al. [10] employed it, in the form of the *Mesh Method of Characteristics*, as the first numerical technique to be employed

in a computer program for this application.

Assuming that the speed distribution distortion is not very high in the cross-section A of the stream thread, the adjustment coefficients a , b and g become the following approximate expressions

$$a = (1 + D \cdot b)^2 \cdot (1 + D), \quad b = (1 + D)^2, \quad (38)$$

$$g = (1 + D \cdot b)^2,$$

where D describes the deviations of the magnitude of the local speed \bar{v} and b the divergence of its direction, both with respect to the average axial speed C . The expressions (38) show that the values of the adjustment coefficients a , b and g converge to one as D approaches zero. If one sets the expressions (38) into equation (34) and these again into the equation (36) one obtains $\lim_{D \rightarrow 0} \mathbf{B}(D) = \mathbf{B}_{1D}$, i.e. in this case the Jacobian matrixes \mathbf{B} and \mathbf{B}_{1D} possess identical eigenvalues (37).

One can determine now the right-eigenvector matrix \mathbf{R}_{1D} of the Jacobian matrix \mathbf{B}_{1D} .

$$\mathbf{R}_{1D} = \begin{bmatrix} 1 & 1 & 1 & 1 \\ C-a & C & C+a & C \\ R_{1D_{31}} & \frac{C^2}{2} & \frac{a^2}{k-1} + \frac{C^2}{2} + C \cdot a & \frac{C}{2} \\ r_i & 0 & r_i & r_i \end{bmatrix} \quad (39)$$

where

$$R_{1D_{31}} = \frac{a^2}{k-1} + \frac{C^2}{2} - C \cdot a$$

Between the Jacobian matrix \mathbf{B}_{1D} , its right-eigenvector matrix \mathbf{R}_{1D} and its inverse matrix \mathbf{R}_{1D}^{-1}

$$\mathbf{R}_{1D}^{-1} = \begin{bmatrix} \frac{C \cdot a + C^2}{k-1} + \frac{C^2}{2} & \frac{-a}{k-1} - C & 1 & 0 \\ \frac{2 \cdot a^2}{k-1} & 0 & 0 & \frac{-2 \cdot a^2}{(k-1) \cdot r_i} \\ -\frac{C \cdot a + C^2}{k-1} + \frac{C^2}{2} & \frac{a}{k-1} - C & 1 & 0 \\ -C^2 & 2 \cdot C & -2 & \frac{2 \cdot a^2}{(k-1) \cdot r_i} \end{bmatrix} \quad (40)$$

one applies

$$\mathbf{R}_{1D}^{-1} \cdot \mathbf{B}_{1D} \cdot \mathbf{R}_{1D} = \mathbf{?}, \quad (41)$$

where $\mathbf{?}$ is the diagonal matrix of the eigenvalues \mathbf{d}_k , with $k = 1 \dots 4$, from equation (37)

$$? = \begin{bmatrix} C-a & 0 & 0 & 0 \\ 0 & C & 0 & 0 \\ 0 & 0 & C+a & 0 \\ 0 & 0 & 0 & C \end{bmatrix}. \quad (42)$$

Note that \mathbf{R}_{1D} diagonalizes the Jacobian matrix \mathbf{B}_{1D} but not \mathbf{B} . One must also note that the product $\mathbf{R}_{j+\frac{1}{2}}^{-1} \cdot \mathbf{F}_{j+\frac{1}{2}}$ influences equation (32) much less when defining the numerical flux $\mathbf{F}_{j+\frac{1}{2}}$ than the sum $\mathbf{F}_j + \mathbf{F}_{j+1}$, since this product is nearly proportional to the difference $\mathbf{F}_j - \mathbf{F}_{j+1}$. This fact shows that the errors caused by application of \mathbf{R}_{1D} instead of \mathbf{R} in the equation (32), will have a low impact on the accuracy of the scheme.

Although at present no exact solution for \mathbf{R} from

$$\mathbf{R}^{-1} \cdot \mathbf{B} \cdot \mathbf{R} = ? \quad (41)$$

is known, one can further reduce the errors mentioned above (with the use of \mathbf{R}_{1D} instead of \mathbf{R}) if

$$\mathbf{R}_{q3D} = \begin{bmatrix} 1 & 1 & 1 & 1 \\ C-a & C & C+a & C \\ R_{q3D_{31}} & a \cdot \frac{C^2}{2} & R_{q3D_{33}} & a \cdot \frac{C^2}{2} \\ r_i & 0 & r_i & r_i \end{bmatrix} \quad (39'')$$

with

$$R_{q3D_{31}} = \frac{a^2}{k-1} + a \cdot \frac{C^2}{2} - C \cdot a$$

$$R_{q3D_{33}} = \frac{a^2}{k-1} + a \cdot \frac{C^2}{2} + C \cdot a$$

and its inverse matrix

$$\mathbf{R}_{q3D}^{-1} = \begin{bmatrix} R_{q3D_{11}}^{-1} & \frac{-a}{k-1} - C & 1 & 0 \\ \frac{2 \cdot a^2}{k-1} & 0 & 0 & \frac{-2 \cdot a^2}{(k-1) \cdot r_i} \\ R_{q3D_{31}}^{-1} & \frac{a}{k-1} - C & 1 & 0 \\ -C^2 & 2 \cdot C & -2 & \frac{2 \cdot a^2}{(k-1) \cdot r_i} \end{bmatrix} \quad (40'')$$

with

$$R_{q3D_{11}}^{-1} = \frac{C \cdot a}{k-1} + (2-a) \cdot \frac{C^2}{2}$$

$$R_{q3D_{31}}^{-1} = \frac{C \cdot a}{k-1} + (2-a) \cdot \frac{C^2}{2}.$$

are used instead of \mathbf{R} and \mathbf{R}^{-1} in the equation (41).

The resulted equation $\mathbf{R}_{q3D}^{-1} \cdot \mathbf{B} \cdot \mathbf{R}_{q3D} = ?$ as nearest

approximation of the equation (41) can be brought into the form

$$\begin{bmatrix} -a + C - w_1 & w_1 & w_1 & w_1 \\ 0 & C & 0 & 0 \\ w_2 & w_2 & a + C + w_2 & w_2 \\ w_3 & w_3 & w_3 & C + w_3 \end{bmatrix} = ? \quad (41'')$$

where

$$w = (k-1) \cdot (1-a) \quad w_1 = \frac{w}{4} \cdot \frac{C^2}{a} \cdot \left(1 - \frac{C}{a}\right)$$

$$w_2 = -\frac{w}{4} \cdot \frac{C^2}{a} \cdot \left(1 + \frac{C}{a}\right) \quad w_3 = \frac{w}{2} \cdot \frac{C^3}{a^2}$$

The following notes are to be made here:

- In the LH member of the equation (41'') only the adjustment coefficient a appears as opposed to in equation (41), i.e., b and g disappear together.
- The equation (41'') is valid only, if w is zero or very small. In fact the magnitude of w is small because a and k are close to one.
- The matrices in the equation (41'') possess an identical determinant, and this happens independently of the a , w and k values.
- The approximation \mathbf{R}_{q3D} is closer to the exact matrix \mathbf{R} from equation (41) than \mathbf{R}_{1D} .

2.2.2. Derivation of the right-eigenvector matrix \mathbf{R} to the position $j + \frac{1}{2}$

Independently of using of \mathbf{R}_{1D} , \mathbf{R}_{q3D} or any other form instead of \mathbf{R} in equation (32) further means

$$\mathbf{R}_{j+\frac{1}{2}} = \mathbf{R} \left(\mathbf{U}_{j+\frac{1}{2}} \right) \quad (43)$$

The vector $\mathbf{U}_{j+\frac{1}{2}}$ can be defined either roughly as the arithmetic average value between \mathbf{U}_j and \mathbf{U}_{j+1} or much more accurately with the help of the so-called average value procedure of Roe [11]. The procedure of Roe supplies the correct average, even if it is applied on different sides of a shock wave or of another discontinuity. Roe's averaged state for the 1D PDE and for a perfect gas for example is discussed in reference [5]. In order to determine Roe's averaged state for the quasi 3D-flow model equation (33) is discretized

$$\mathbf{F}_{j+\frac{1}{2}} - \mathbf{F}_{j-\frac{1}{2}} = \bar{\mathbf{B}} \cdot \left(\mathbf{U}_{j+\frac{1}{2}} - \mathbf{U}_{j-\frac{1}{2}} \right). \quad (44)$$

The components of the Jacobian matrix $\bar{\mathbf{B}}$ are now the averaged values of the state variables. The vectorial equation (44) contains four scalar equations. The first one is easily fulfilled. In order to be able to process the other three scalar equations, the following positive auxiliary parameter has to be introduced

$$e = \sqrt{\frac{\mathbf{r}_{j+\frac{1}{2}} \cdot \mathbf{A}_{j+\frac{1}{2}}}{\mathbf{r}_{j-\frac{1}{2}} \cdot \mathbf{A}_{j-\frac{1}{2}}}}. \quad (45)$$

Two solutions result for the axial speed from the second scalar equation of (44) at the position $j \pm \frac{1}{2}$

$$C_{j+\frac{1}{2}} = \frac{C_j + e \cdot C_{j+1}}{1 + e} \quad (46)$$

$$C_{j+\frac{1}{2}} = \frac{C_j - e \cdot C_{j+1}}{1 - e}. \quad (46')$$

From these there is the benefit that (46) have not unsteadiness (because $e > 0$) and for this reason further only it is applied.

From the third scalar equation of (44) it results for the averaged value of the specific total enthalpy

$$h_{j+\frac{1}{2}} = \frac{h_j + e \cdot h_{j+1}}{1 + e} + \frac{a}{2} \cdot \left(\mathbf{k}_{j+\frac{1}{2}} - 1 \right) \cdot \frac{1 + e}{e} \cdot \frac{C_j - e \cdot C_{j+1}}{C_j - C_{j+1}} \cdot C_{j+\frac{1}{2}}^2 \quad (47)$$

where for a perfect gas there is defined as follows

$$h = \frac{\mathbf{k}}{\mathbf{k} - 1} \cdot \frac{p}{r} + a \cdot \frac{C^2}{2} = \frac{a^2}{\mathbf{k} - 1} + a \cdot \frac{C^2}{2}. \quad (48)$$

Equation (47) may be applied only in the case $C_j - C_{j+1} \neq 0$. Otherwise, i.e. when $C_j - C_{j+1} = 0$, the unsteadiness from the equation (47) is to be treated accordingly. For example

$$h_{j+\frac{1}{2}} = \frac{h_j + e \cdot h_{j+1}}{1 + e} + \frac{a}{2} \cdot \left(\mathbf{k}_{j+\frac{1}{2}} - 1 \right) \cdot \frac{1 + e}{e} \cdot C_{j+\frac{1}{2}}^2. \quad (47')$$

Note here that expression (47') represents the exact Roe's averaged specific total enthalpy only if $e = 1$.

With help of (47) and (48) one can now also determine Roe's averaged value of the local speed of sound

$$a_{j+\frac{1}{2}}^2 = \left(\mathbf{k}_{j+\frac{1}{2}} - 1 \right) \cdot \left(h_{j+\frac{1}{2}} - \frac{a}{2} \cdot C_{j+\frac{1}{2}}^2 \right). \quad (49)$$

The fourth scalar equation of (44) provides Roe's averaged value of the mass fraction of a gas component

$$r_{ij+\frac{1}{2}} = \frac{r_{ij} + e \cdot r_{ij+1}}{1 + e}.$$

Nevertheless, one question still remains unanswered: Which value does $\mathbf{k}_{j+\frac{1}{2}}$ take? As an example one supposes the following situation:

Inside the inlet valve port there is only pure air, thus there the fraction of the exhaust gases (index E) is $r_{E_{\text{int.ake}}} = 0$. Inside the cylinder are only exhaust gases and thus the share of the exhaust gases is $r_{E_{\text{cyl}}} = 1$. If the inlet valve would open and the pressure of the exhaust gases in the cylinder would be higher than in the intake pipe (the temperature normally likewise), then the exhaust gases flow from the cylinder into the inlet valve port. One can imagine in this situation that the air and exhaust gases do not mix themselves immediately and completely and thus a discontinuity in the fluid composition in the intake pipe between j and $j+1$ occurs, where $r_{E_j} = 0$ (only air) and $r_{E_{j+1}} = 1$ (only exhaust gases). For deriving

$$\mathbf{k}_{j+\frac{1}{2}} = \frac{c_p \left(T_{j+\frac{1}{2}}, r_{E_{j+\frac{1}{2}}} \right)}{c_p \left(T_{j+\frac{1}{2}}, r_{E_{j+\frac{1}{2}}} \right) - R_G \left(r_{E_{j+\frac{1}{2}}} \right)} \quad (50)$$

one must first determine the specific isobaric thermal capacity $c_p \left(T_{j+\frac{1}{2}}, r_{E_{j+\frac{1}{2}}} \right)$ for the ideal gas mixture, where for example

$$T_{j+\frac{1}{2}} = \frac{a_{j+\frac{1}{2}}^2}{\mathbf{k}_{j+\frac{1}{2}} \cdot R_G \left(r_{E_{j+\frac{1}{2}}} \right)}. \quad (51)$$

One can see that the state variables from equation (47), (49), (50) and (51) depend on each another. For example the total enthalpy, the isentropic exponent, the temperature and the speed of sound can be determined at the same time by an iterative calculation. In order to achieve the convergence, one or two iterations would be suffi-

cient, if as initial value e.g., the arithmetic average values of the temperature or of the isentropic exponent between j and $j+1$ will be used.

Now all necessary state variables for calculation of $R_{j+\frac{1}{2}}$ are available.

2.2.3. Derivation of the vector \mathbf{F} at the position $j+\frac{1}{2}$

The final term of the equation (32), the vector \mathbf{F} is explained in what follows. For a second order upwind TVD scheme the components f_k of the vector \mathbf{F} are [5]

$$f_{k, j+\frac{1}{2}} = s \left(d_{k, j+\frac{1}{2}} \right) \cdot (m_{k, j+1} + m_{k, j}) - y \left(d_{k, j+\frac{1}{2}} + x_{k, j+\frac{1}{2}} \right) \cdot q_{k, j+\frac{1}{2}}. \quad (52)$$

The function s for a variable z is

$$s(z) = \frac{1}{2} \cdot (y(z) - 1 \cdot z^2), \quad (53)$$

where the function

$$y = \begin{cases} |z| & \text{if } |z| \geq e_1 \\ \frac{z^2 + e_1^2}{2 \cdot e_1} & \text{if } |z| < e_1 \end{cases} \quad (54)$$

expresses the adjustment for the fulfillment of the entropy balance concerning the variable z (s. [5] for more details).

For example, for an unsteady flow the parameter $e_1 = 0$ is recommended, i.e.

$$y(z) = |z|. \quad (54')$$

In the equation (52) the variables q_k are the components of the vector

$$\mathbf{T}_{j+\frac{1}{2}} = \mathbf{R}_{j+\frac{1}{2}}^{-1} \cdot (\mathbf{U}_{j+1} - \mathbf{U}_j), \quad (55)$$

and the function x is

$$x_{k, j+\frac{1}{2}} = s \left(d_{k, j+\frac{1}{2}} \right) \begin{cases} \frac{m_{k, j+\frac{1}{2}} - m_{k, j}}{q_{k, j+\frac{1}{2}}} & \text{if } q_{k, j+\frac{1}{2}} \neq 0 \\ 0 & \text{if } q_{k, j+\frac{1}{2}} = 0 \end{cases}. \quad (56)$$

The function m is a so-called limiter in the TVD method and can be selected in different variations, e.g.

$$\mu_{k, j} = \minmod \left(q_{k, j-\frac{1}{2}}, q_{k, j+\frac{1}{2}} \right), \quad (57)$$

where the *minmod* function for two variables x and y is defined as

$$\minmod(x, y) = \text{sgn}(x) - \max(0, \min(|x|, y \cdot \text{sgn}(x))) \quad (58)$$

and $\text{sgn}(x)$ denotes the sign of the variable x .

In case of a high-resolution Lax-Friedrichs scheme the function y becomes simple

$$y = \frac{1}{1}. \quad (54')$$

2.3. Treatment of the non-homogeneous PDE (26)

For the integration of the non-homogeneous PDE (26) - that describes a so-called *problem containing source terms* - a splitting method is used.

2.3.1. Processing of the source term \mathbf{H}

The processing of the source vector \mathbf{H} from the equation (26.3) is the same as for the vector \mathbf{F} shown already above. The Jacobian matrix \mathbf{D} of the vector

$$\mathbf{H}(\mathbf{U}) = \begin{bmatrix} -U_1 \cdot \left(\frac{A_t}{A} + \frac{U_2}{U_1} \cdot \frac{A_x}{A} \right) \\ -U_2 \cdot \left[\left(\frac{A_t}{A} + \mathbf{b} \cdot \frac{U_2}{U_1} \cdot \frac{A_x}{A} \right) + \frac{1}{2} \cdot \frac{\mathbf{I}_D}{D_H} \cdot \frac{|U_2|}{U_1} \right] \\ H_3 \\ -U_4 \cdot \left(\frac{A_t}{A} + \frac{U_2}{U_1} \cdot \frac{A_x}{A} \right) \end{bmatrix} \quad (59)$$

with

$$H_3 = \left[- \left(\frac{A_t}{A} + \mathbf{k} \cdot \frac{U_2}{U_1} \cdot \frac{A_x}{A} \right) - \frac{4 \cdot k}{D_H} \cdot \frac{k-1}{U_1 \cdot R_G} \right] \cdot \left(U_3 - \frac{\mathbf{g}}{2} \cdot \frac{U_2^2}{U_1} \right) - \frac{1}{2} \cdot \frac{U_2^2}{U_1} \cdot \left[\left(\mathbf{g} \cdot \frac{A_t}{A} + \mathbf{a} \cdot \frac{U_2}{U_1} \cdot \frac{A_x}{A} \right) - \frac{\mathbf{I}_D}{D_H} \cdot \frac{|U_2|}{U_1} \right] + \frac{4 \cdot k}{D_H} \cdot T_W$$

is

$$\mathbf{D} = \begin{bmatrix} -\frac{A_t}{A} & -\frac{A_x}{A} & 0 & 0 \\ D_{21} & D_{22} & 0 & 0 \\ D_{31} & D_{32} & D_{33} & 0 \\ r_i \cdot C \cdot \frac{A_x}{A} & -r_i \cdot \frac{A_x}{A} & 0 & -\left(\frac{A_t}{A} + C \cdot \frac{A_x}{A}\right) \end{bmatrix}, \quad (60)$$

where

$$D_{21} = \left(\mathbf{b} \cdot \frac{A_x}{A} + \frac{1}{2} \cdot d_2 \right) \cdot C^2,$$

$$D_{22} = -d_2 \cdot C - \left(\frac{A_t}{A} + 2 \cdot \mathbf{b} \cdot C \cdot \frac{A_x}{A} \right),$$

$$D_{31} = \left(\mathbf{k} \cdot C \cdot \frac{A_x}{A} + d_3 \right) \cdot \left(d_1 - \mathbf{g} \cdot \frac{C^2}{2} \right) + \left(\mathbf{a} \cdot \frac{A_x}{A} - d_2 \right) \cdot C^3,$$

$$D_{32} = \left(\frac{3}{2} \cdot d_2 \cdot C + \mathbf{g} \cdot d_3 \right) \cdot C + \left[-\mathbf{k} \cdot d_1 + \left(\mathbf{k} \cdot \mathbf{g} - \frac{3}{2} \cdot \mathbf{a} \right) \cdot C^2 \right] \cdot \frac{A_x}{A},$$

$$D_{33} = -\left(\frac{A_t}{A} + \mathbf{k} \cdot C \cdot \frac{A_x}{A} \right) - d_3,$$

$$d_1 = \frac{1}{\mathbf{k} - 1} \cdot \frac{p}{r},$$

$$d_2 = \frac{1_D}{D_H} \cdot \text{sgn}(C),$$

$$d_3 = \frac{4 \cdot k}{D_H} \cdot \frac{\mathbf{k} - 1}{r \cdot R_G}.$$

2.3.2. Application of the first step of the predictor-corrector method

In this step only the temporal change of the state vector \mathbf{U} caused by the source vector \mathbf{H} is considered during the first temporal half step width, i.e., from the PDE (26) only $\mathbf{U}_t = \mathbf{H}$ remains. The Euler discretization for the first temporal half step width now supplies

$$\frac{\mathbf{U}_j^{n+\frac{1}{2}} - \mathbf{U}_j^n}{\frac{Dt}{2}} = \frac{\mathbf{H}_j^{n+\frac{1}{2}} + \mathbf{H}_j^n}{2}. \quad (62)$$

Furthermore, the change of the state vector \mathbf{U} after the first step (high index l) becomes

$$D\mathbf{U}_j^l = \mathbf{U}_j^{n+\frac{1}{2}} - \mathbf{U}_j^n = \frac{Dt}{4} \cdot \left(\mathbf{H}_j^{n+\frac{1}{2}} + \mathbf{H}_j^n \right). \quad (63)$$

In order to be able to determine it, one must first deter-

mine the source vector \mathbf{H} at the time $n + \frac{1}{2}$. For this purpose its differential

$$d\mathbf{H}(\mathbf{U}) = \left(\frac{d}{d\mathbf{U}} \mathbf{H}(\mathbf{U}) \right) \cdot d\mathbf{U} = \mathbf{D}(\mathbf{U}) \cdot d\mathbf{U} \quad (64)$$

is discretized on the time axis for a half step width

$$\mathbf{H}_j^{n+\frac{1}{2}} = \mathbf{H}_j^n + \mathbf{D}_j^n \cdot \left(\mathbf{U}_j^{n+\frac{1}{2}} - \mathbf{U}_j^n \right) = \mathbf{H}_j^n + \mathbf{D}_j^n \cdot D\mathbf{U}_j^l. \quad (65)$$

If one now inserts the equation (65) into (63) and resolves it after $D\mathbf{U}$ one gets

$$D\mathbf{U}_j^l = \frac{Dt}{2} \cdot \left(\mathbf{E} - \frac{Dt}{4} \cdot \mathbf{D}_j^n \right)^{-1} \cdot \mathbf{H}_j^n, \quad (66)$$

and thus after the first step of the predictor-corrector method

$$\mathbf{U}_j^l = \mathbf{U}_j^n + D\mathbf{U}_j^l, \quad (67)$$

where the exponent -1 in equation (66) denotes the inverse of the matrix resulted in the brackets.

2.3.3. Application of the second step of the predictor-corrector method

Now only the integration of the homogeneous PDE (27) on the total temporal step width Dt is accomplished, where in equation (30) \mathbf{U}^l is inserted instead of the state vector \mathbf{U}^n

$$\mathbf{U}_j^{ll} = \mathbf{U}_j^l - \mathbf{I} \cdot \left(\mathbf{F}_{j+\frac{1}{2}}^l - \mathbf{F}_{j-\frac{1}{2}}^l \right). \quad (68)$$

2.3.4. Application of the third step of the predictor-corrector method

Now, in this final step again only the change of the state vector \mathbf{U} caused by the source vector \mathbf{H} during the second temporal half step width is considered

$$D\mathbf{U}_j^{ll} = \frac{Dt}{2} \cdot \left(\mathbf{E} - \frac{Dt}{4} \cdot \mathbf{D}_j^{ll} \right)^{-1} \cdot \mathbf{H}_j^{ll}, \quad (69)$$

and thus at the time $n+1$ the following results after the complete application of the predictor-corrector method

$$\mathbf{U}_j^{n+1} = \mathbf{U}_j^{ll} + D\mathbf{U}_j^{ll}. \quad (70)$$

3. PRESENTATION OF THE SIMULATION RESULTS AND THEIR COMPARISON WITH THE MEASUREMENTS

3.1. Data of the experimental engine and arrangement of the measuring points

For validating the simulation results a "AVL 520" one-cylinder research engine of the laboratory for Power Engineering, Piston and Turbo Machines of the University of Applied Sciences Hamburg was used. Some engine data can be taken out of the following table and Figure 1.

Bore	Stroke	Vol. Comp. Ratio
120 mm	120 mm	15.85

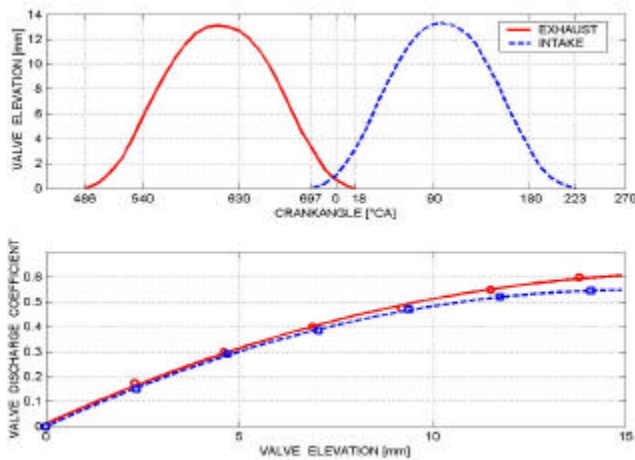


Figure 1: Valve elevation and valve discharge coefficient curves of the AVL 520 engine

The quasi-3D method introduced above is now applied to the simulation of the gas exchange processes. The simulation results and the pressure measurements are presented here only for the flow in the intake pipe. The arrangement of all measuring points is represented in the Figure 2.

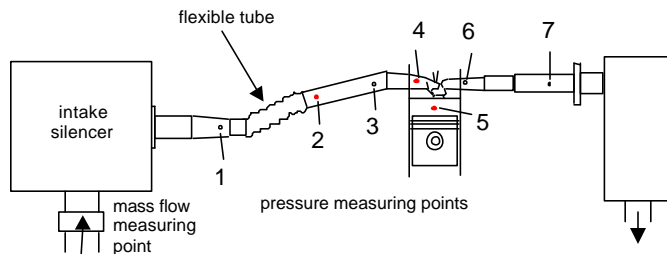


Figure 2: Arrangement of all measuring points.

The comparisons between the simulation results and pressure measurements in the intake pipe are done only for measuring points 2 and 4 for space reasons. The measurements were accomplished in several series and partially repeated, first of all, because of the limited number of only four input channels of the pressure indicating system and, second, for accuracy reasons [6].

Figure 3 shows the 3D computing mesh of the intake pipe and intake port segment, i.e., between the flexible joint tube and the inlet valve (s. Figure 2), where some typical cross-sections and pressure measuring points are marking.

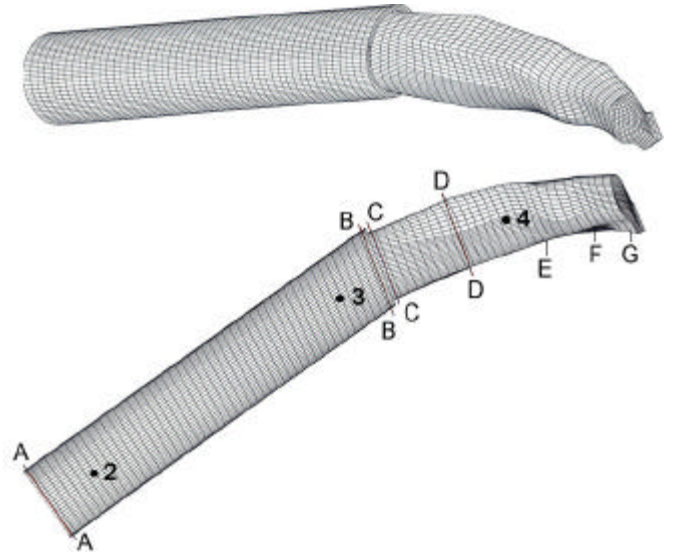
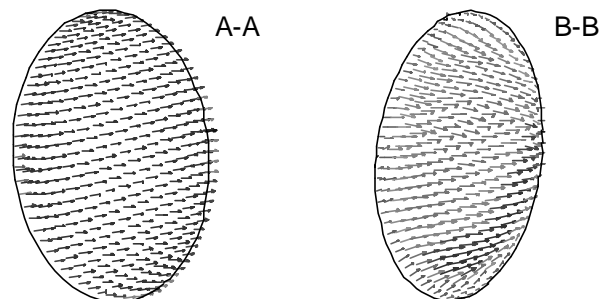


Figure 3: Intake pipe segment and inlet port mesh with typical cross-sections and pressure measuring points.

3.2. Computing of the adjustment coefficients

For computing of the adjustment coefficients a , b and g the 3D-flow simulation program STAR CD is used. This simulation is accomplished only for a compressible turbulent stationary forward and reverse airflow through the intake pipe and inlet port. The flow speed vectors in the cross-sections mentioned above are represented in Figure 4.



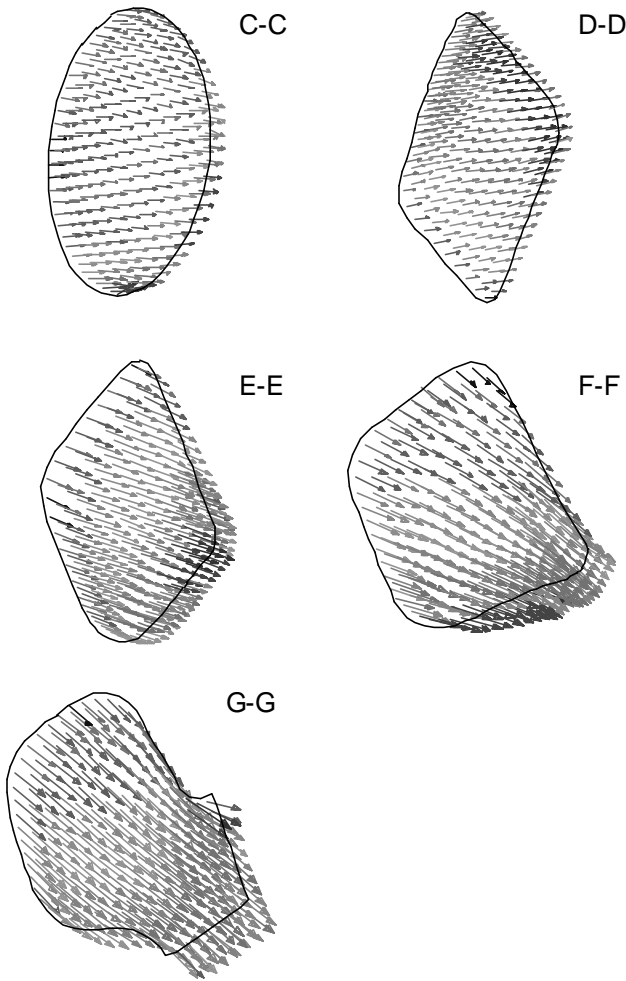


Figure 4: Flow speed vectors in the cross sections shown in Figure 3.

Using these simulation results and the definition of the adjustment coefficients from the equations (13), (18) and (19) one obtains the variations from Figure 5 for the adjustment coefficients a , b and g .

3.3. Comparison between simulations and measurements and between quasi-3D and 1D simulation methods

The adjustment coefficients are now used in quasi-3D simulation as input data; therefore the simulation of unsteady compressible flow can be accomplished.

Since the start conditions in the pipes and cylinder are unknown when simulation is starting, they are arbitrarily selected. In this case several operating cycles must be simulated in each stationary operating point of the engine (constant speed and load). Thus the start conditions in pipes and in the cylinder are renewed by the final states of the previous operating cycle in order to achieve the convergence.

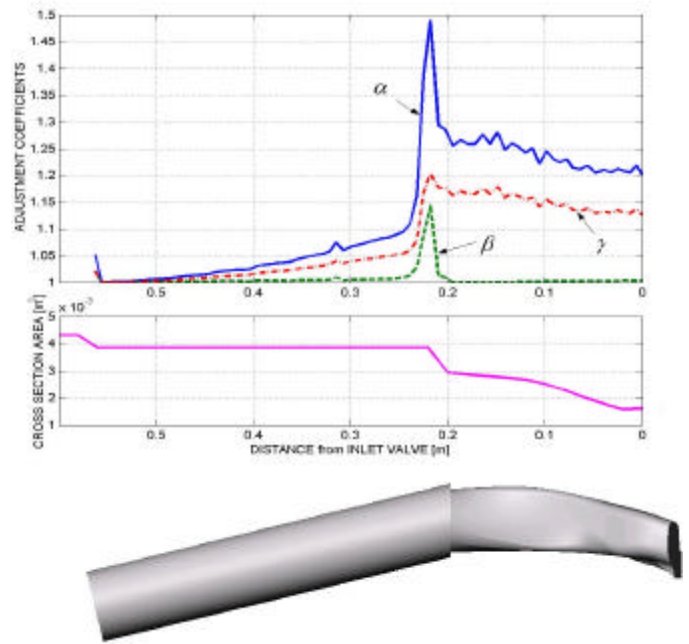


Figure 5: Adjustment coefficients a , b and g along the intake pipe segment for the stationary forward flow.

In order to allow the comparison with the experiments, the environment conditions present during the measurement and the engine speed are used as input data for the simulations. The comparisons are done in several engine-operating points (EOP) as in Figure 6.

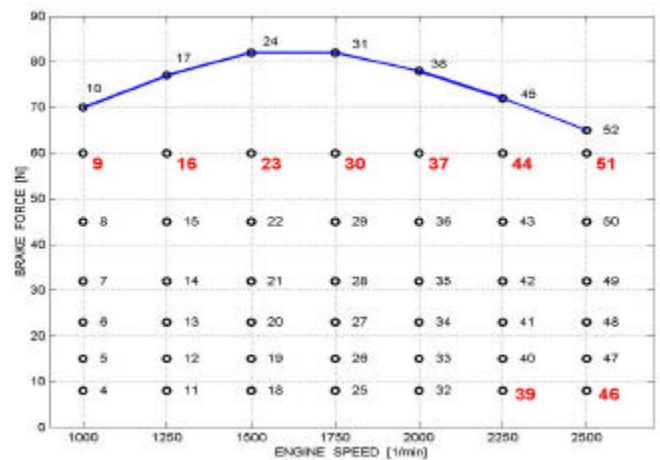


Figure 6: Engine operating points (EOP) map

The analysis of all pressure variations at the measuring points 2 and 4 displayed in the Appendix shows good agreement between simulations and experiments. Some minor differences occur in any EOP because:

- a) the supplementary (disregarded in model) wall vibration, wall elasticity and wall friction due to the flexible joint tube between the measuring points 1 and 2 (s. Figure 2),
- b) only the intake pipe segment from Figure 3 and Figure 5, i.e. between the flexible joint tube and inlet valve, is simulated with the quasi-3D method and the remainder with the 1D method, and
- c) no other local loss coefficients for the entire intake pipe (quasi-3D segment and 1D remainder) are used in this case.

Note that the combination from b) is chosen here first for easier comparison of the simulation methods, and second because only within this segment it is meaningful to insert the interface to the true-3D model. For this reason the differences between quasi-3D and 1D simulation results originate (only) from the influence of the adjustment coefficients from Figure 5.

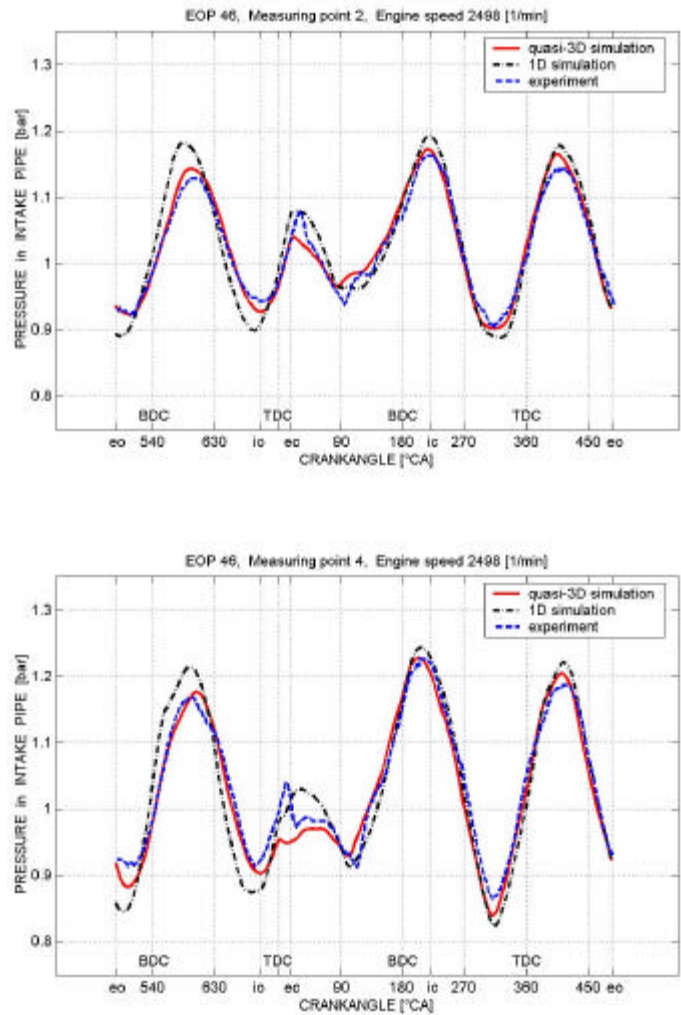


Figure 7: Comparisons between quasi-3D and 1D simulation methods by EOP 46.

Two comparisons between 1D (with adjustment coefficients $a, b, g = 1$) and quasi-3D (with the adjustment coefficients from Figure 5) simulation methods are made by EOP 46 (s. Figure 7) and 51 (s. Figure 8).

The comparison shows that the quasi-3D model works better and closer to the experiments and that without any adapted local loss coefficients. Although the improvement seems to be small, one must note here (because of the simplicity of the intake pipe geometry) that even the 1D method works in this case quite well. On the other hand only a segment of this pipe is treated here with the quasi-3D method as mentioned.

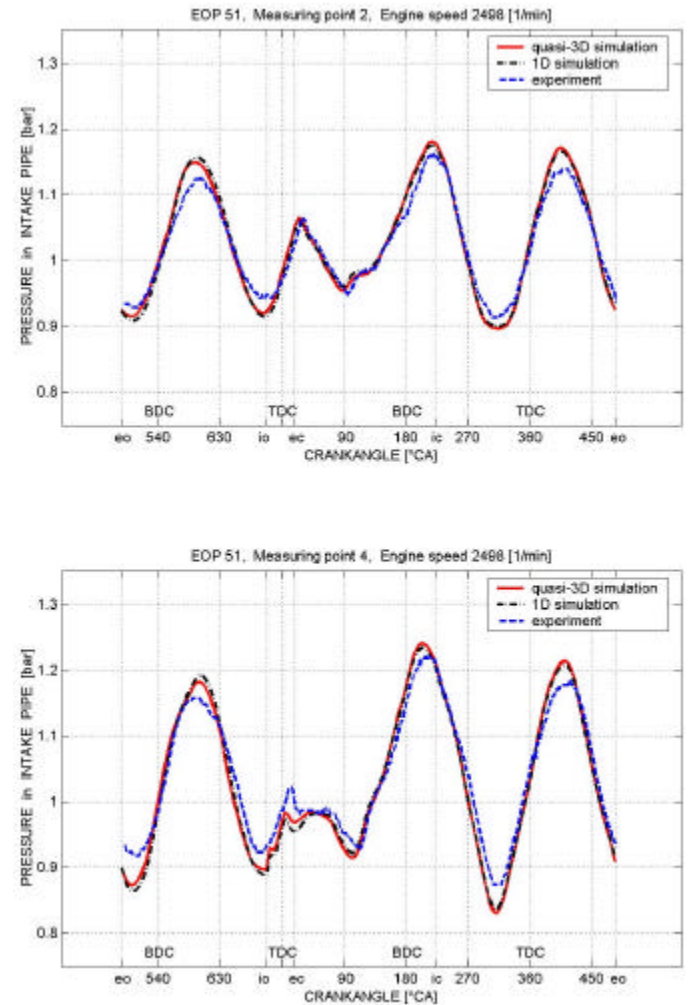


Figure 8: Comparisons between quasi-3D and 1D simulation methods by EOP 51.

One expects that the differences between quasi-3D and 1D simulations will be more significant in case of complicated pipe geometry, pipe junctions and manifolds.

The quasi-3D method allows one to take into consideration the real distribution of losses along the pipes (as curvatures, asymmetry of the pipes and channels etc). On

the contrary the 1D method requires artificial concentration of the distributed losses in some cross sections, which are treated during the simulation as discontinuity interfaces or boundaries [12]. On one hand, the treatment of the boundaries is very time-consuming and causes convergence problems frequently. On the other hand the simulation results are inaccurate close to the boundaries. This fact becomes more critical because of the complexity of modern manifolds, which requires inserting a series of boundaries along a pipe.

CONCLUSION

The quasi-3D method is introduced here as a compromise between the 1D and true-3D methods. This new method improves the quality of the 1D-simulation results noticeably, without increasing the cost of computation proportionally.

The quasi-3D method is suited for two application kinds:

1. It can be used only for the accurate simulation of manifold flow processes for providing the flow velocity, pressure, density and gas composition in the cylinder interfaces needed in the true-3D cylinder process simulations.
2. This method can be employed as a more accurate solution compared with the classical 1D method for gas exchange process simulations of ICE.

The first application type closes the development loop. Such a closed loop may be composed of CAD-design, exported geometry, mesh generation, stationary true-3D simulation, adjustment coefficient computation, instationary quasi-3D simulation, instationary true-3D simulation, results evaluation and again CAD-design. The use of the quasi-3D method in such a development loop permits to take into consideration the refined geometry of the manifolds better as before and therefore to reduce considerably the measurement efforts and development costs.

The second application type is natural. One must conclude that for the treatment of multipipe junctions with the quasi-3D method an appropriate procedure is needed. The adjustment coefficients must be computed in this case for all flow possibilities (flow direction and some flow rates) through these multipipe junctions, i.e., the stationary true-3D simulation must be carried out several times. This expense remains still low because in this stationary simulation only the exit boundary conditions are changed and the computing time makes no difference in this case. The accuracy gain of the quasi-3D method will be important because of the use of appropriate adjustment coefficients, which take into consideration the refined real geometry of these multipipe junctions.

For even better accuracy it is recommended to compute the adjustment coefficients for some forward and reverse

flow rates through all the pipes.

REFERENCES

1. Zierep, J., *Grundzüge der Strömungslehre*, Springer Verlag (German), 1997
2. Boussinesq, I., *Memoire sur l'influence des frottements dans les mouvements réguliers des fluides*, J. de math. pur et appl., nr. 13, p. 377, (French) 1868
3. Florea, J., Panaitescu, V., *Mecanica fluidelor*, EDP-Bucuresti (Romanian), 1979
4. Idelchik, I. E., *Handbook of hydraulic-resistance*, Springer Verlag, 1986
5. Yee, H.-C., *A class of high resolution explicit and implicit shock capturing methods*, NASA Technical memorandum of 101088 and of Karman Institutes for Fluid Dynamics, Lecture Series 1989-04
6. Schillmueller, J., *Experimental investigation of the gas exchange processes at a AVL one-cylinder research engine*, Graduate paper at the University of Applied Sciences Hamburg (German), 1997
7. Riemann, B., *Über die Fortpflanzung ebener Luftwellen von endlicher Schwingungsweite*, Gott. Abh. 8 (Math.) 43-65 (German), 1858/59
8. Jenny, E., *One-dimensional transient flow with consideration of friction, heat transfer and charge of section*, Brown Boveri Rev. 37, 447-461, 1950
9. Seifert, H., *Instationäre Strömungsvorgänge in Rohrleitungen an Verbrennungskraftmaschinen*, Springer Verlag (German), 1962
10. Benson, R. S., Garg, R.D., and Woollatt, D., *A numerical solution of unsteady flows problems*, Int. J. Mech. Sci., 6, 117-144, 1964
11. Roe, P. L., *Approximate Riemann solvers, parameter vectors and difference schemes*, J. Comp. Phys., Vol. 43. 357-372, 1981
12. Winterbone, D. E., Pearson, R. J., *Design techniques for engine manifolds - Wave action methods for IC engines*, Professional Eng. Publishing, 1999

CONTACT

Prof. Dr. Eng. Victor Gheorghiu

University of Applied Sciences
Dep. of Mechanical Engineering
Berliner Tor 21, 20099 Hamburg, Germany
http://www.victor_gheorghiu.de
<mailto:grg@rzbt.fh-hamburg.de>

APPENDIX

In the Appendix, only the pressure variations comparison at the measuring points 2 and 4 (s. Figure 2 and Figure 3) at seven engine speeds are presented. Presented supplementary are the pressure, flow speed, density and exhaust gas volume fraction variations as 3D-diagrams, i.e. as isometric illustrations in the distance-crankangle (distance-time) plane. In all these 3D-diagrams the sur-

face of the state variable (e.g. the pressure) as well auxiliary variations are presented according to the notations from Figure 9.

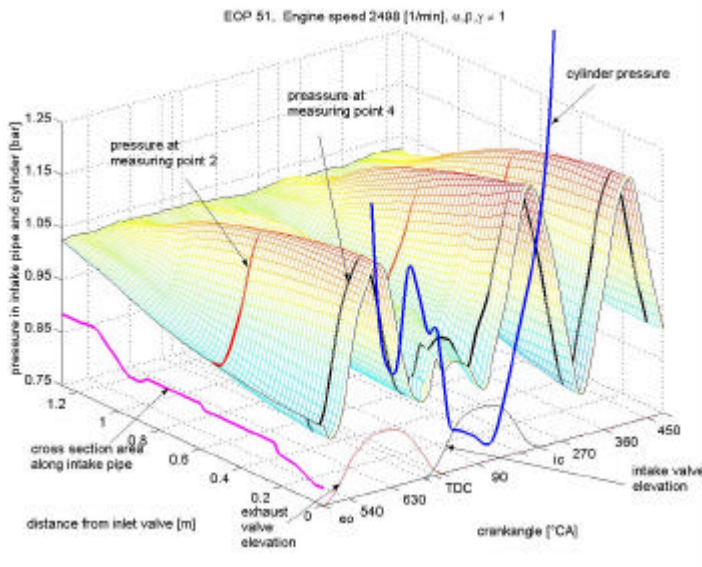


Figure 9: 3D-diagram of a state variable (here pressure) in the intake pipe as an isometric illustration in the distance-crankangle (distance-time) plane.

The 3D-diagrams of the exhaust gas volume fraction (EGVF) show the back flows within intake pipe perfectly, and so one can find out when and how intensive these back flows occur. For example the back flows during the valve overlap are missing at EOP 39 and 44, are moderate at EOP 09 and 30, and are strong at EOP 16, 23, 37, 46 and 51. The explanation for the back flows can be found, if one analyzes the 2D- and 3D-diagrams of the intake pressure. The 3D-diagrams for the density show a valley (because of the high exhaust gas temperature) when the back flows occur, while the 3D-diagrams of the flow velocity show negative values.

A second back flow could appear when the inlet valve is closing if the cylinder pressure exceeds the intake pipe pressure. This occurrence can be observed at all presented EOP. The intensity of this second back flow can be captured once again from the 3D-diagrams of the exhaust gas volume fraction (EGVF). The 3D-diagrams of the flow velocity and density only confirm these occurrences.

For the ICE with extern gas mixture formation (for example, MPI gasoline engines) it is useful to have the 3D-diagrams of the flow velocity one's disposal. With its help one can optimize for example the location choice of the gasoline injectors and the intake pipe shape. If supplementary a gasoline spray model is added and a new state variable as gas component for the gasoline vapor mass fraction is introduced, one can perform this tuning even better.

